ACCOUNTS of chemical research

Article

Cite This: Acc. Chem. Res. 2019, 52, 2684−2693

pubs.acs.org/accounts

Exciton Spatial Coherence and Optical Gain in Colloidal Two-Dimensional Cadmium Chalcogenide Nanoplatelets

Qiuyang Li and Tianquan Lian*

Department of Chemistry, Emory University, 1515 Dickey Drive Northeast, Atlanta, Georgia 30322, United States

CONSPECTUS: Two-dimensional (2D) cadmium chalcogenide (CdX, X = Se, S, Te) colloidal nanoplatelets (NPLs) make up an emerging class of quantum well materials that exhibit many unique properties including uniform quantum confinement, narrow thickness distribution, large exciton binding energy, giant oscillator strength, long Auger lifetime, and high photoluminescence quantum yield. These properties have led to their great performances in optoelectrical applications such as lasing materials with a low threshold and large gain coefficient. Many of these properties are determined by the structure and dynamics of band-edge excitons in these 2D materials. Motivated by fundamental understanding of both 2D nanomaterials and their applications, the properties of 2D excitons have received intense recent interest. This Account provides an overview of three key properties of 2D excitons: how big is the 2D exciton (i.e., exciton center-of-mass coherent area); how the exciton moves in 2D NPLs (i.e., exciton in-plane transport mechanism); how multiple excitons interact with each other (i.e., biexciton Auger recombination); and their effects on the optical gain mechanism and threshold of colloidal NPLs.

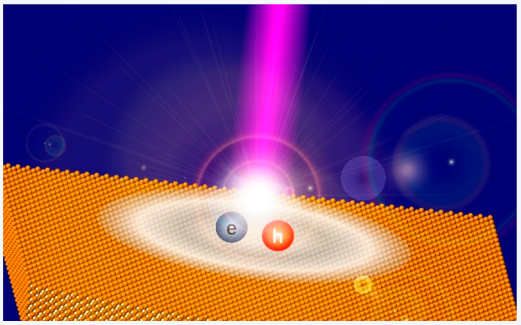

After a brief introduction in Section 1, the current understandings of 2D electronic structures of cadmium chalcogenide NPLs, and type-I CdSe/CdS and type-II CdSe/CdTe core/crown NPL heterostructures are summarized in Section 2. Section 3 discusses the direct measurement of exciton center-of-mass coherent area in 2D CdSe NPLs, its dependence on NPL parameters (thickness, lateral area, dielectric environment, and temperature), and the resulting giant oscillator strength transition (GOST) effect in 2D NPLs. 2D exciton diffusive in-plane transport in CdX NPLs and the comparison of exciton transport mechanisms in 2D NPLs and 1D nanorods are reviewed in Section 4. How Auger recombination lifetime depends on nanocrystal dimensions in NPLs, quantum dots, and nanorods is discussed in Section 5. The lateral area and thickness dependent Auger recombination rates of NPLs are shown to be well described by a model that accounts for the different dependence of the Auger recombination rates on the quantum confined and nonconfined dimensions. It is shown that Auger recombination rates do not follow the "universal volume scaling" law in 1D and 2D nanocrystals. Section 6 describes optical gain mechanisms in CdSe NPLs and the dependence of optical gain threshold on NPL lateral size, optical density, and temperature. The differences of optical gain properties in 0D−2D and the bulk materials are also discussed, highlighting the unique gain properties of 2D NPLs. At last, the Account ends with a summary and perspective of key remaining challenges in this field in Section 7.

1. INTRODUCTION

Cadmium chalcogenide (CdX, X = Se, S, Te) colloidal two-dimensional (2D) nanoplatelets (NPLs) or quantum wells (QWs) make up a new class of quantum-confined nanocrystals (NCs).[1,2] Compared to 0D quantum dots (QDs) and 1D nanorods (NRs), 2D NPLs have tunable and atomically precise thicknesses, leading to a uniform quantum confinement energy.[1] The thickness distribution in their ensembles is narrow so that the emission line-width of a NPL ensemble is almost the same as that of a single NPL (∼42 meV),[3] which is sharper than the best-reported core/shell QDs (∼67 meV).[4] The basal plane of 2D NPLs is well passivated by ligands,[5] which reduces surface defects and results in a photoluminescence (PL) quantum yield (QY) of over 50% in NPLs without any passivating inorganic shell layers.[1,5] Moreover, the multiexciton lifetime of cadmium chalcogenide NPLs (hundreds of ps)[6,7] is longer than that of QDs (10s of ps) of similar exciton transition energy.[8] These properties have led to reports of promising lasing performances with large gain coefficients and low thresholds.[7,9−15] The best reported amplified spontaneous emission (ASE) threshold of CdSe NPLs is as low as ∼6 μJ/cm^2,[7] which is over an order of magnitude lower than that in QDs with similar band-edge exciton transition energies.[16,17]

The lasing performance and optical gain (OG) properties of 2D NPLs are mainly determined by their absorption and emission properties, which are controlled by the properties of 2D excitons (Scheme 1). Strong quantum- and dielectric-confinement effects of 2D NPLs give rise to a large exciton binding energy of ∼100−200 meV.[1,18] This strongly bound electron−hole pair enhances the band-edge transition strength. It is speculated that, in the absence of exciton−phonon scattering and surface imperfection, the exciton center-of-mass

Received: May 12, 2019
Published: August 21, 2019

DOI: 10.1021/acs.accounts.9b00252
Acc. Chem. Res. 2019, 52, 2684−2693

Scheme 1. Physical Properties of 2D Excitons in CdSe NPLs: Coherent Area, Transport, Auger Annihilation, and Optical Gain by Multiexciton Emission

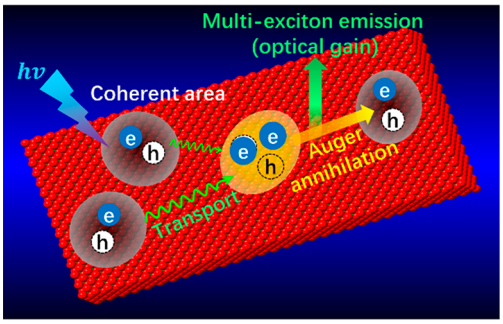

can coherently delocalize throughout the entire NPL, giving rise to the giant oscillator strength transition (GOST) effect.[1,19−21] The area of exciton center-of-mass directly determines the radiative decay rate of NPLs,[19,22] exciton in-plane transport mechanisms (diffusive vs ballistic),[23,24] and multiexciton annihilation rates.[25] In recent years, 2D exciton and OG properties of NPLs and their heterostructures have been intensively studied because of the interests in both the fundamental understanding of 2D nanomaterials and improvement of their lasing performances.

This Account provides an overview of the current understanding of three key 2D exciton properties (exciton center-of-mass coherence area, exciton transport and Auger recombination) in colloidal CdX (X = S, Se, Te) NPLs and how these properties affect their optical gain mechanisms. The remainder of this Account starts with a summary of the current understanding of 2D electronic structures of NPLs and the band alignments of type-I and type-II NPL heterostructures. The direct measurement of exciton coherent area of 2D CdSe NPLs and the GOST effect is discussed in Section 3. 2D exciton diffusive in-plane transport and biexciton Auger recombination in NPLs are reviewed in Sections 4 and 5, respectively. The dependence of the OG threshold on NPL lateral size, optical density, and temperature is discussed in Section 6. The Account ends with a summary of current status and a perspective of key challenges of this field.

2. ELECTRONIC STRUCTURE OF NPLS AND NPL HETEROSTRUCTURES

CdX (X = Se, S, and Te) NPLs have a zinc-blend structure with alternating Cd and X layers and with Cd on both the top and bottom basal planes.[1] They are often referred to as *n* CdX monolayer (ML) NPLs, which contain *n* + 1 Cd and *n* X layers. TEM images of these NPLs show nearly rectangular shape with length and width of 10s to 100s of nm (Figure 1a−c).[6] The electronic structure of NPLs is reflected by their absorption spectra (Figure 1d),[6] with the two lowest energy absorption peaks representing the electron-heavy hole (A exciton) and electron-light hole (B exciton) transitions, respectively. The A and B excitonic transition energies can be quantitatively reproduced by an eight-band effective-mass approximation method.[1] The positions of the conduction band (CB) and valence band (VB) edge are determined by their bulk band-edge positions, electron ($E_{k(e)}$) and hole ($E_{k(e)}$) quantum confinement energies, carrier self-image energy induced by the dielectric confinement effect, and exciton binding energy induced by the electron−hole Coulomb interaction.[1] A tight-binding calculation has shown that the self-image energy and the exciton binding energy are both enhanced by the dielectric confinement effect and have similar values (∼100−200 meV) but opposite signs.[18] As a result, the CB (VB) edge positions for 3, 4, and 5 ML CdSe NPLs can be calculated to be −3.20 eV (−5.87 eV), −3.41 eV (−5.82 eV), and −3.53 eV (−5.79 eV), respectively, versus vacuum level by just considering the quantum confinement effect (Figure 1e).[6]

NPL heterostructures can be formed by growing two different NPLs together and exhibit two possible types of band alignments: (1) type-I band alignment, where both CB and VB edges of one NPL are within the band gap of the other, and (2) type-II band alignment, where CB and VB edges of

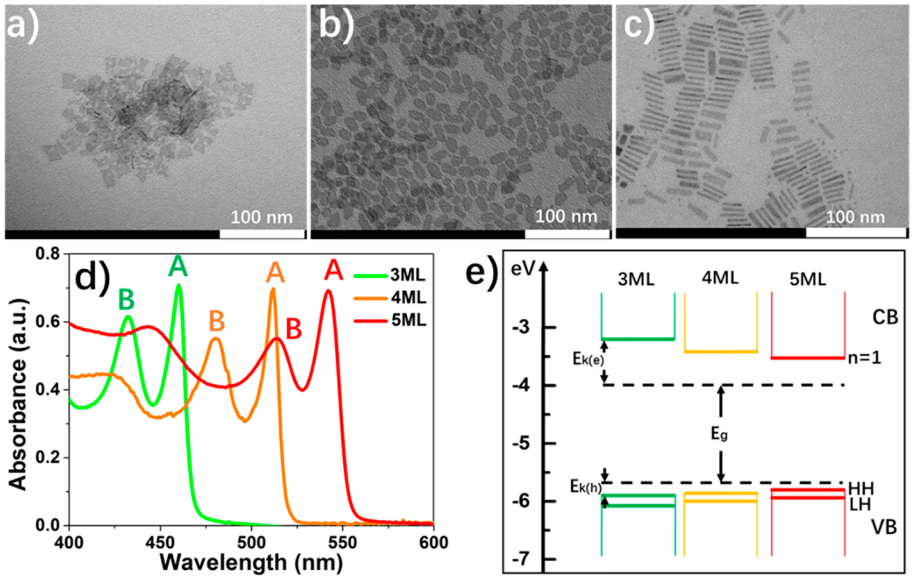

Figure 1. Transmission electron microscopy (TEM) images of (a) 3 ML, (b) 4 ML, and (c) 5 ML CdSe NPLs. (d) Absorption spectra of 3−5 ML CdSe NPLs. (e) Schematic of conduction and valence band-edge levels of 3−5 ML CdSe NPLs and bulk CdSe. Panels a−e are adapted with permission from ref 6. Copyright 2017 American Chemical Society.

DOI: 10.1021/acs.accounts.9b00252
Acc. Chem. Res. 2019, 52, 2684−2693

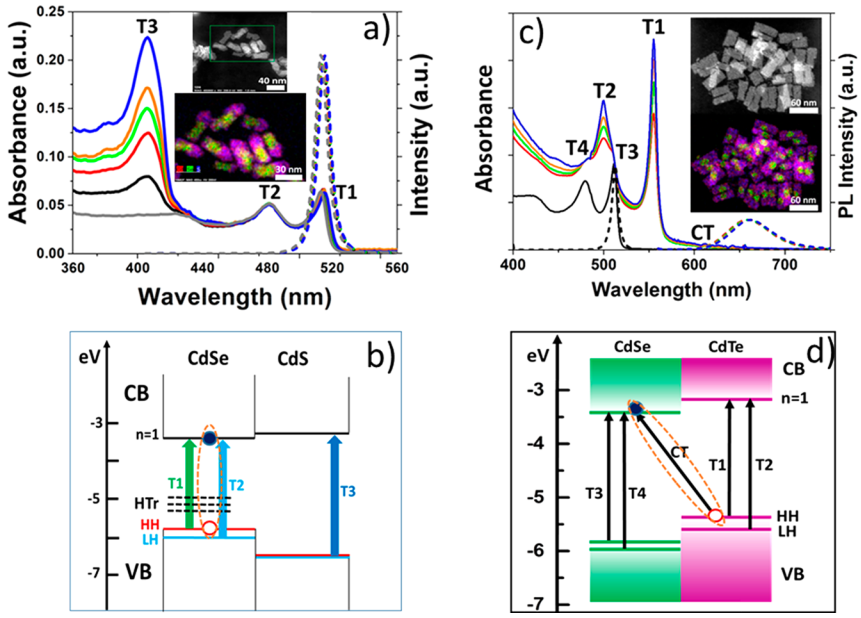

Figure 2. Core/crown NPL heterostructures (a) Absorption spectra of CdSe/CdS core/crown (CC) NPLs with different crown sizes. Inset: the high angle annular dark field (HAADF) scanning TEM (STEM) image (upper panel) and the energy-dispersive X-ray (EDX) image (lower panel) of CdSe/CdS CC NPLs. (b) Scheme of band alignment and band-edge transitions of type-I CdSe/CdS CC NPLs. (c) Absorption spectra of free CdSe NPLs and CdSe/CdTe CC NPLs with different crown sizes. Inset: HAADF-STEM image (upper panel) and the EDX image (lower panel) of CdSe/CdTe CC NPLs. (d) Scheme of band alignment and band-edge transitions of type-II CdSe/CdTe CC NPLs. Panels a and b are adapted with permission from ref 23. Copyright 2016 American Chemical Society. Panels c and d are adapted with permission from ref 24. Copyright 2017 American Chemical Society.

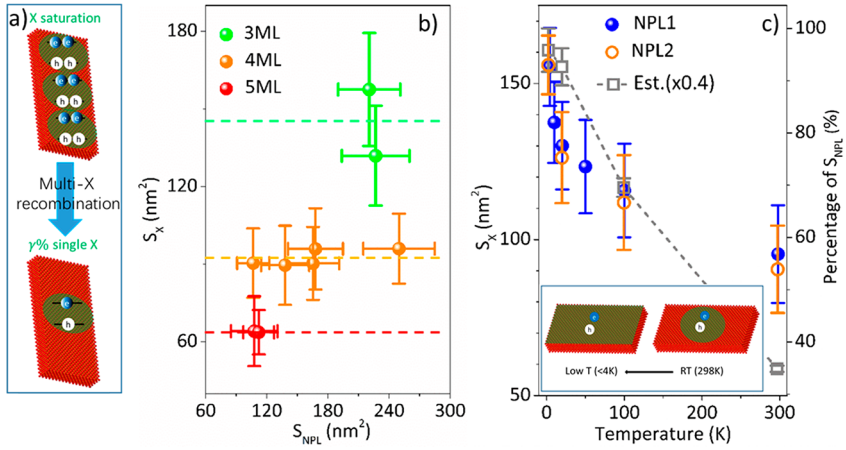

Figure 3. Coherent area of exciton center-of-mass. (a) Scheme of decay from the initial multiexciton state with a saturated number of band-edge excitons to a long-lived single exciton state in CdSe NPLs. (b) Exciton coherent area (S_X) of 3−5 ML CdSe NPLs as a function of NPL lateral area. (c) Experimentally determined S_X (blue spheres and orange circles) and the estimated S_X (gray squares) of 4 ML CdSe NPLs as a function of temperature. Inset: scheme of exciton center-of-mass coherent extension at 298 K and 4K. Panels a−c are adapted with permission from ref 21. Copyright 2019 American Chemical Society.

two NPLs stagger with respect to each other. Core/crown (CC) NPL heterostructures are formed by extending an NPL crown laterally around an NPL core with the same number of monolayers. Extending CdS around CdSe NPLs forms type-I CC NPLs (Figure 2a).[23,26] The absorption of CdSe/CdS CC NPLs is the sum of absorption of CdSe and CdS NPLs, and their PL spectra (dashed lines in Figure 2a) are all consistent with the CdSe core emission, indicating the formation of type-I heterostructure (Figure 2b).[23,26] Similarly, extending CdTe around CdSe NPLs forms type-II CC NPLs and their absorption is dominated by the absorption of CdSe and CdTe NPLs (Figure 2c).[12,24,27−29] However, CdSe/CdTe CC NPLs emit at ∼660 nm, different from the emissions in CdSe core (∼515 nm) or CdTe crown (∼550 nm), and show an additional absorption feature below the CdTe band gap These features can be attributed to the charge-transfer (CT) exciton state formed at the core/crown interface, with the electron in CdSe and the hole in CdTe due to their type-II band alignment (Figure 2d).[24,27]

3. COHERENT EXCITON CENTER-OF-MASS DELOCALIZATION AND GOST EFFECT

With uniform quantum confinement energy, exciton center-of-mass coherent spatial area (S_X) can extend within 2D NPL,

DOI: 10.1021/acs.accounts.9b00252
Acc. Chem. Res. 2019, 52, 2684−2693

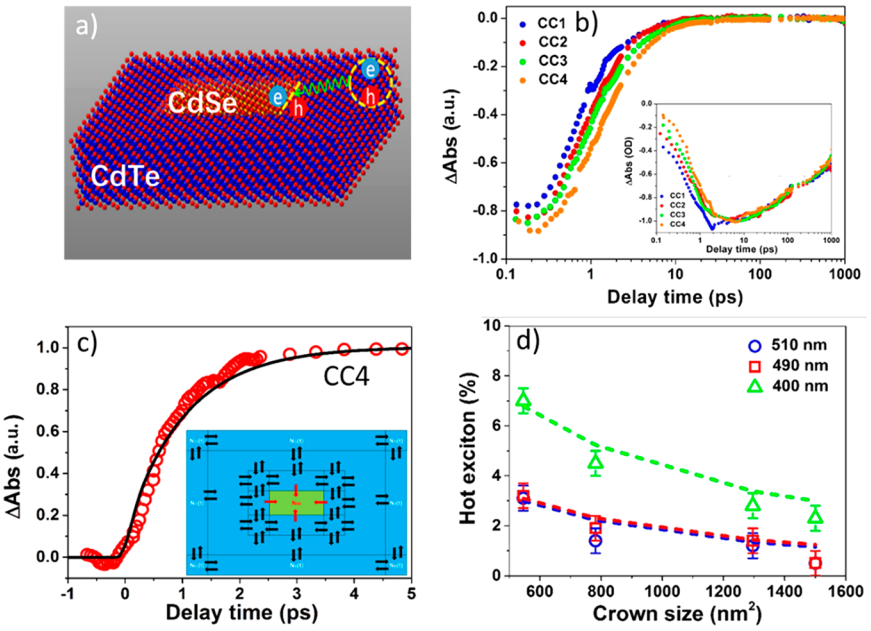

Figure 4. Exciton transport in core/crown heterostructures. (a) Scheme of the exciton core-to-crown in-plane transport in CdSe/CdTe type-II core/crown (CC) NPL heterostructures. (b) Normalized CdTe exciton bleach kinetics of CC1−4. Inset: normalized charge-transfer exciton bleach kinetics of CC1−4. (c) Normalized charge-transfer exciton kinetics (red circles) and a fit according to a 2D diffusion model (solid line) of CC4. Inset: scheme of the 2D diffusion model for exciton transport. (d) Measured percentage of hot exciton transport in CC1−4 as a function of crown size at different pump wavelengths (open symbols) and fit according to the 2D diffusion model (dashed line). Panles a−d are adapted with permission from ref 24. Copyright 2017 American Chemical Society.

which increases the exciton transition oscillator strength, giving rise to the GOST effect.[1,19,20] This effect can also be understood in the k-space because the coherent extension of center-of-mass in the real space corresponds to concentrating exciton center-of-mass momentum at the Γ-point in k-space. The GOST effect affects the absorption,[30] emissions,[22] lasing,[21] and transport[23,24] properties of NPLs. Despite its importance, S_X is mostly unknown in colloidal NPLs and other 2D materials because experimental techniques to measure this quantity directly are lacking. It should be noted that this quantity differs from exciton Bohr's radius, which has been determined in 1D and 2D materials.[31,32] So far, evidence to support the GOST effect comes mainly from the observation of temperature[1,20] and size dependent[22] band-edge exciton radiative decay rates in NPLs because they are proportional to the oscillator strength of the exciton transition.[19] Ithurria et al. reported an accelerated PL decay with decreasing temperature of 5 ML CdSe NPLs due to the GOST effect: the PL half-life decreases from ∼3990 ps at 300 K to ∼340 ps at 6 K.[1] Similarly, Naeem et al. reported a temperature dependent band-edge exciton radiative decay in 4 ML CdSe NPLs with a lifetime <1 ps at 5 K using transient resonant four-wave mixing.[20] However, the large variation of reported exciton radiative lifetimes (from 100s of ps[1] to < 1ps[20] at 5−6 K) makes the characterization of the GOST effect difficult. In a study of the NPL lateral area dependent PL decay rates, Ma et al. observed that the decay rate becomes independent of size when the NPL lateral area exceeds ∼160 nm^2, which represents an upper limit of the exciton center-of-mass coherent area in NPLs.[22]

Recently, a method to directly measure the S_X of CdSe NPLs in solution via pump fluence dependent TA spectroscopy was reported.[21] At a high enough pump fluence, all band-edge excitons for each NPL are excited. Thus, under the saturation pump fluence, the band-edge exciton absorbance of the excited region ($X(t_E)$) at early delay time (t_E, 1−2 ps), prior to any exciton annihilation and charge recombination processes, is proportional to the whole NPL lateral area, S_{NPL} (upper panel of Figure 3a). At long delay times (t_L, 800−1000 ps), all multiexcitons have been annihilated, and only single excitons remain in the excited NPLs.[6,21] Therefore, the band-edge exciton absorbance of the excited region at t_L, $X(t_L)$, is proportional to the exciton coherent area (S_X) of single excitons: γS_X (lower panel of Figure 3a). γ represents the percentage of excited NPL population remains at the excited state at t_L under single exciton conditions, which can be determined independently. This relationship can be represented as

$$\frac{X(t_E)}{X(t_L)} = \frac{S_{NPL}}{\gamma S_X} \quad (1)$$

$X(t_E)$ and $X(t_L)$ can be extracted by fitting the TA spectra at t_E and t_L, respectively,[21] and S_{NPL} is the NPL lateral area determined from their TEM images.

Using this method (eq 1), the S_X of 3−5 ML CdSe NPLs is reported to be lateral area independent but decreases with NPL thickness, indicating that the extent of coherent delocalization of exciton center-of-mass increases with the degree of quantum confinement (Figure 3b).[21] It is interesting to note that in thinner NPLs, the exciton binding energy increases, which leads to smaller Wannier-Mott exciton radii (shorter relative distance between electron and hole).[18] This result suggests that the extent of quantum confinement lead to opposite effects on the size of excitons in the center-of-mass and internal coordinates. Figure 3c shows that the S_X of 4 ML CdSe NPLs increases from ∼95 nm^2 at 298 K to ∼150 nm^2 at 4K, indicating the exciton coherent area extends to the whole NPL at low temperature (4K), directly supporting the

DOI: 10.1021/acs.accounts.9b00252
Acc. Chem. Res. 2019, 52, 2684−2693

GOST effect (inset of Figure 3c). Despite the uniform confinement energy expected from the atomically precise NPL thickness, the exciton−phonon scattering can reduce the spatial coherence of excitons: $S_X = 4h^2/\Delta(T)M$, where h is the Planck's constant, $\Delta(T)$ is the transition line width at temperature (T), and M is the sum of the effective masses of electron and hole at the band-edge.[19,22] The estimated S_X values here (~160 nm^2, gray squares in Figure 3c) and in the previous study[22] are larger than our experimentally determined S_X of 4 ML CdSe NPLs (~90 nm^2) but are close to that of 3 ML CdSe NPLs (~144 nm^2). This indicates that the spatial coherent area of exciton center-of-mass is enhanced by stronger quantum confinement and is reduced by other factors in addition to exciton−phonon scattering.

4. DIFFUSIVE EXCITON IN-PLANE TRANSPORT

Because of a lack of quantum confinement in the lateral dimension, excitons and carriers can move laterally within NPLs. Thus, the mechanism of in-plane exciton and carrier transport processes is important to the understanding of multiexciton annihilation,[6,25] exciton dissociation and long-distance charge (electron and hole) transfer,[33,34] which are key processes in NC-based photocatalysis systems.[34−36] Previous reports of CdSe NPLs[25] or nanobelts[37] suggest a ballistic exciton transport mechanism.[25,37] However, other studies have shown that excitons in 2D quantum wells with an active layer of few nanometers are sandwiched by two barrier layers transport diffusively at room temperature.[38−41] CC NPL heterostructures provide an ideal model for exciton in-plane transport study. As discussed in Section 2, excitons in the crown are driven to the core (core/crown interface) according to type-I (type-II) band alignment, and this crown-to-core (or interface) transport process can be captured and quantified by TA spectroscopy. In this section, recent studies of exciton transport in both CdSe/CdS[23] and CdSe/CdTe CC NPLs are discussed.[24]

To examine exciton transport mechanisms, the dependences of exciton transport rate and efficiency on the crown size were studied in four CdSe/CdTe CC NPLs with the same CdSe core and increasingly larger CdTe crown size (labeled as CC1−4).[24] As shown in Figure 4a, the excitons created at the CdTe crown are transported to the core/crown interface to form long-lived charge-transfer excitons due to the type-II band alignment in these heterostructures. It has been shown that the exciton bleach signals of the CdTe crown probe its CB edge electron population, while the bleach at charge-transfer exciton band probes the CB edge electron population in the CdSe core.[24] The decay of CdTe exciton bleach kinetics (Figure 4b) agrees well with the growth of charge-transfer exciton kinetics (inset of Figure 4b), confirming that the CB electron is transferred from the CdTe crown to CdSe core. Considering the large exciton binding energy in cadmium chalcogenide NPLs,[1,18] the electron−hole pair is thought to move together as a quasi-particle. Thus, this electron transfer process reflects the exciton crown-to-interface transport process. The comparison of CC1−4 (Figure 4b) shows that the crown-to-core exciton transport process becomes faster in smaller crowns, excluding the ballistic transport mechanism. The charge-transfer exciton kinetics can be well reproduced by a 2D exciton diffusion model (black solid line in Figure 4c). This 2D diffusion model assumes that the excitons are randomly distributed at the CdTe crown and undergo 2D diffusion motion until they encounter the CdSe core, at which they become interface localized charge-transfer excitons. This 2D diffusion problem can be solved numerically to obtain the kinetics of exciton populations at CdTe crown and CdSe core (Figure 4c).[24] The good agreement between the simulated and measured kinetics suggests that excitons are transported by diffusive motions in the CdTe crown.

The contribution of hot excitons to the transport process in CdSe/CdTe CC NPLs at room temperature was also examined. CC NPLs were excited at different wavelengths (530, 510, 490, and 400 nm) to generate CdTe excitons with different excess energies. Because only band-edge (cold) excitons contribute to exciton bleach signal, the contribution of hot exciton transport can be calculated from $1 - A_{ini}$ (A_{ini} is the initial amplitudes of exciton bleach). The result shows that hot exciton contribution increases with excitation energy up to ~7 to ~2% at 400 nm excitation from CC1 to CC4 (Figure 4d). Detailed analysis (dashed lines in Figure 4d) reveals that the effective diffusion constant of hot excitons is larger than that of cold excitons and increases with the excitation energy.[24] It is interesting to note that exciton transport in CC NPLs differs from previously reported multiple-quantum-well (MQW) materials grown by molecular beam epitaxy, where cold exciton diffusion dominates at room temperature.[38−41] The difference may results from the much smaller lateral dimension of NPLs (10s of nm) than MQW materials (100s of nm to a few micrometers): the time scale of exciton transport is comparable to that of the hot exciton relaxation in NPLs, increasing the contribution of hot exciton transport.[24] A similar 2D diffusion model also applies to CdSe/CdS CC NPLs,[23] and the diffusion constant of band-edge (cold) excitons at room temperature was determined to be ~2.2 and ~2.5 cm^2/s for CdS[23] and CdTe NPLs,[24] respectively.

It is interesting to compare exciton diffusion in 2D NPLs and 1D NRs. The diffusion constant for CdS NPLs is similar to that of CdS NRs (~2.3 cm^2/s),[42] but smaller than that of bulk CdS (~3.2 cm^2/s), which is likely due to the extra scattering channels induced by the large surface area of NPL nanostructures.[42] Compared with CdSe/CdS dot-in-rod (DIR) heterostructures, which shows a rod length dependent exciton rod-to-dot transport efficiency with lower efficiencies in longer rods,[42] both CdSe/CdS and CdSe/CdTe CC NPLs show crown size independent exciton crown-to-core (interface) transport efficiencies.[23,24] This is because exciton trap states are randomly distributed on CdS rod surfaces so that exciton trapping probability increases with the rod length.[42] In contrast, trap states in 2D NPLs are concentrated on the edges (or the core/crown interface in CC heterostructures) with the basal planes well passivated with organic ligands (e.g., oleic acid),[5] leading to the crown area independent exciton trapping process. Because of fast exciton in-plane transport, near unity exciton transport efficiency in CdSe/CdTe CC NPLs has been reported.[24] It should be noted that recently, Pandya et al. reported that the exciton in-plane transport efficiency depends sensitively on the lateral size of CdSe/CdTe CC NPLs and the quality of core/crown interfaces.[43] The origin for different NPL size dependences remains unclear.

5. MULTIEXCITON ANNIHILATION

Multiexciton annihilation is a key efficiency limiting factor in many optoelectrical applications of NCs such as light-emitting diodes (LED),[44,45] lasing,[10,14] and multiexciton generation process.[46] Nonradiative Auger recombination dominates the multiexciton annihilation process and is enhanced in NCs as

DOI: 10.1021/acs.accounts.9b00252
Acc. Chem. Res. 2019, 52, 2684−2693

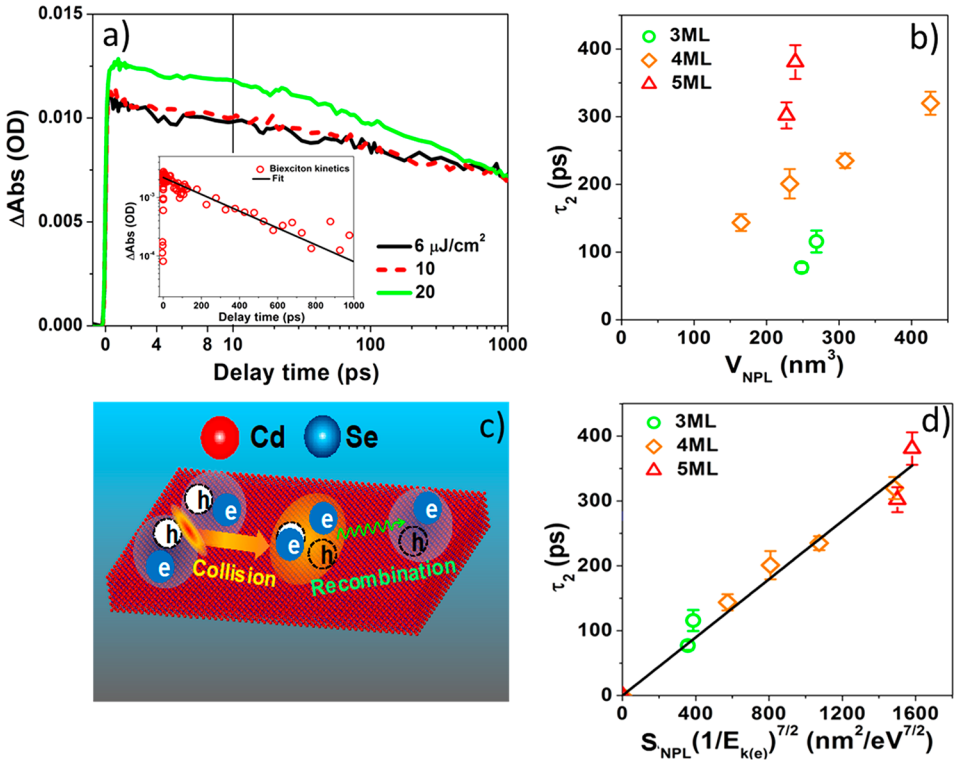

Figure 5. Area and thickness dependent biexciton Auger recombination in NPLs. (a) Normalized A exciton kinetics of 5 ML CdSe NPLs at low pump fluence (<20 μJ/cm^2). Inset: extracted biexciton decay kinetics (circles) with the single-exponential fit (black line). (b) Biexciton lifetime of 4−5 ML CdSe NPLs as a function of NPL volume (V_{NPL}). (c) Scheme of two-step Auger recombination model in CdSe NPLs. (d) Biexciton lifetime of CdSe NPLs as a function of the product of NPL lateral area (S_{NPL}) and $E_{k(e)}$ to the −7/2 order. The black line is the linear fit. Panels a−d are adapted with permission from ref 6. Copyright 2017 American Chemical Society.

the quantum confinement effect relaxes the requirement of momentum conservation.[8,47−49] Previous studies on 0D QDs have shown that the biexciton Auger recombination lifetime scales linearly with the QD volume in both indirect- and direct-gap semiconductors, following a "universal volume scaling law".[8,50] More recently, the biexciton lifetime of PbSe NRs was also reported to scale linearly with NR volume.[48] This observation is surprising considering the very different natures of carrier motions in the quantum confined and nonconfined dimensions. Thus, more systematic studies are needed to test the applicability of the "universal volume scaling law" beyond 0D materials and unveil the dependence of Auger recombination in 1D NRs and 2D NPLs.[6]

The thickness and lateral area dependence of biexciton Auger recombination have been recently reported.[6] A comparison of A exciton kinetics normalized at 800−1000 ps (Figure 5a) shows that the kinetics are independent to pump fluence at <10 μJ/cm^2, indicating that they are dominated by single exciton decay, but contain additional biexciton decay components at >20 μJ/cm^2. The biexciton kinetics is then extracted by subtracting single-exciton kinetics (at 6 μJ/cm^2) from total exciton kinetics (at 20 μJ/cm^2) (inset of Figure 5a). Biexciton decays single-exponentially with a time constant of ∼380 ps, which is much shorter than the single-exciton radiative lifetime divided by 2 (∼5 ns),[1] indicating that nonradiative Auger process dominates the biexciton decay in CdSe NPLs and the biexciton lifetime can be approximated as the biexciton Auger recombination time.[25,51] Using this method to extract biexciton lifetime, very different biexciton lifetimes are observed in CdSe NPLs with similar volume (∼250 nm^3) but different thicknesses (Figure 5b), breaking the "universal volume scaling law". This indicates different dependence of Auger lifetime on quantum- (thickness) and nonquantum-confined (lateral area) dimensions in CdSe NPLs.

To account for the different dependence of Auger lifetime on the lateral and thickness dimensions, a new model for Auger recombination in 2D NPLs was proposed (Figure 5c). Because of the large diffusion constant of ∼220−250 nm^2/ps (as discussed in Section 4),[23,24] excitons can diffuse throughout the whole NPL with a lateral area of ∼220 nm^2 within ∼1 ps, which indicates frequent collisions of biexcitons (with a collision frequency, F_C) prior to Auger recombination on the 100s of ps time scale (Figure 5b). Assuming an Auger recombination probability per collision (P_{Aug}), the biexciton Auger recombination rate ($1/\tau_2$) can be represented as the product of F_C and P_{Aug}: $1/\tau_2 = F_C P_{Aug}$. F_C is proportional to the exciton density, which is proportional to the reciprocal of NPL lateral area ($1/S_{NPL}$) according to a 2D binary exciton collision model.[52] P_{Aug} is reported to be determined by the quantum confined energy of CB edge electron ($E_{k(e)}$) in quantum wells with similar band structures.[53] Thus, biexciton lifetime is given by this relationship:

$$\frac{1}{\tau_2} = F_C P_{Aug} \propto \frac{1}{S_{NPL}} (E_{k(e)})^{7/2} \quad (2)$$

Figure 5d shows that the biexciton lifetime of different NPLs scales linearly with $S_{NPL}(E_{k(e)})^{-7/2}$ according to eq 2, confirming the proposed new Auger recombination model. This model should apply to other 1D and 2D materials: the nonquantum-confined dimension determines the exciton

DOI: 10.1021/acs.accounts.9b00252
Acc. Chem. Res. 2019, 52, 2684−2693

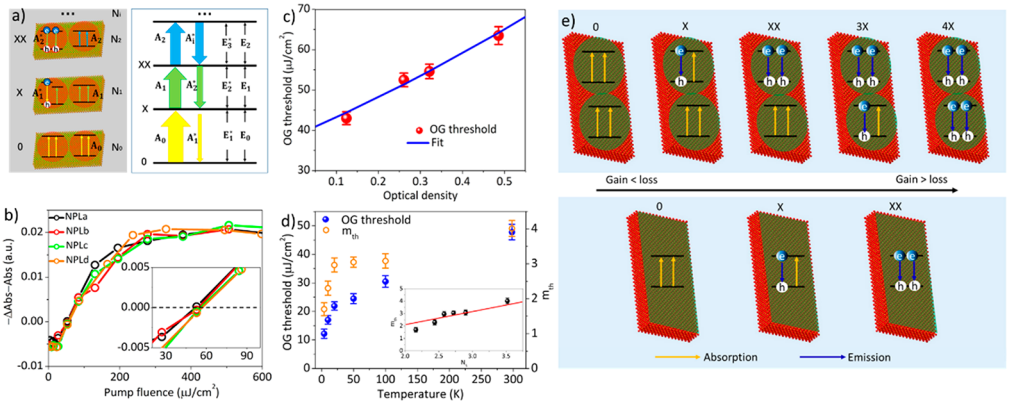

Figure 6. Optical gain in NPLs. (a) States and transitions involved in biexciton optical gain of CdSe NPLs in single particle (left panel) and exciton state representations (right panel), respectively. N_0 (0), N_1 (X), and N_2 (XX) are probabilities (and labels) of NPL states with 0, 1, and 2 excitons, respectively. Colored arrows represent different band-edge transitions with different energies. (b) OG maximum amplitude as a function of pump fluence of NPLa–d. Inset: the same results at low pump fluence (20–100 $\mu J/cm^2$). (c) OG threshold of 4 ML CdSe NPLs as a function of optical density at the excitation wavelength (400 nm). (d) OG threshold and the average exciton number per NPL at the OG threshold (m_{th}) of 4 ML CdSe NPLs in hexane as a function of temperature. Inset: m_{th} of 4 ML CdSe NPLs as a function of the saturation number of the band-edge exciton (N_S). Red line is a linear fit. (e) Scheme of different exciton states in NPLs at room temperature with the saturation number of the band-edge exciton (N_S) of 4 (upper panel) and 2 (lower panel). Panels a–c are adapted with permission from ref 57. Copyright 2018 Royal Chemical Society. Panels d and e are adapted with permission from ref 21. Copyright 2019 American Chemical Society.

collision frequency, and the quantum-confined dimension determines the Auger probability per collision.[54]

Despite the progress discussed above, how Auger recombination depends on nanocrystal dimensions remains an open question. A 100-fold difference on the biexciton lifetime of 4 ML CdSe NPLs has been reported in the literature.[6,7,25,55] She et al. reported a lateral area independent biexciton lifetime of 4 and 5 ML CdSe NPLs, which differs from the work discussed above.[55] Different mechanisms for lateral dimension dependent Auger lifetime are also reported. Rabani and co-workers reported a "length scaling" law of biexciton lifetimes for 1D CdSe NRs.[56] In their model, the length-dependence of biexciton Auger recombination rate results from the length dependent overlap between the biexciton and final exciton state wave functions without considering exciton diffusion and collision. Moreover, Pelton et al. reported that the Auger lifetime of CdSe/CdS core/shell NPLs changes with the shell thickness nonmonotonically,[49] consistent with a previous theoretical prediction for core/shell QDs.[53] These results suggest that much more systematic studies of Auger recombination mechanisms in 1D and 2D are still needed.

6. OPTICAL GAIN PROPERTIES OF CDSE NPLS

Two-dimensional cadmium chalcogenide NPLs have shown great potentials for lasing applications, exhibiting large gain coefficients and low optical gain (OG) threshold.[7,9−15,55] Understanding OG properties of 2D NPLs benefits the rational design and improvement of NPL-based lasers. Different from 0D QDs, where excitons are confined in all three dimensions, excitons in 2D NPLs are free to move in the plane, which increase the degree of degeneracy of band-edge exciton states and may alter their OG properties. This section reviews recent studies of the OG threshold of CdSe NPLs, especially its dependence on lateral size, optical density (OD), and temperature.

As shown in Figure 6a, in colloidal NPL solution, OG is achieved when the total emission from NPL species is larger than their total absorption. NPL species with different exciton states (0, X, and XX for NPLs with 0, 1, and 2 excitons, respectively) absorb and emit different number of photons. Therefore, OG threshold is determined by the relative population of different NPL species (N_0, N_1, and N_2 for NPLs with 0, 1, and 2 excitons, respectively) and can be determined by pump fluence dependent TA spectroscopic study.[57] In a TA measurement, the optical density of samples under illumination is given by $\Delta Abs(\lambda,t) + Abs(\lambda)$ (λ is the wavelength), where the first term is the pump-induced absorbance change shown in TA spectra and the second is the static absorbance before pump. OG is achieved when the gain (stimulated emission, $-\Delta Abs(\lambda,t)$) is larger than loss (absorption, $Abs(\lambda)$): $-\Delta Abs(\lambda,t) - Abs(\lambda) > 0$. Figure 6b shows the OG peak ($-\Delta Abs(\lambda,t) - Abs(\lambda)$) maximum amplitude as a function of pump fluence of 4 ML CdSe NPLs with different lateral areas (labeled as NPLa–d with increasing lateral areas), and the intercept on the x-axis represents the OG threshold fluence. To enable the comparison of NPLs samples of different lateral areas, their optical density at the pump wavelength (400 nm) was controlled to the same value to ensure the same number of absorbed photons, and NPL lateral area independent OG threshold was observed (inset of Figure 6b). Comparison of the same CdSe NPL samples with different optical density (by changing the concentration of the NPL sample solution) at the pump wavelength (400 nm) shows that the OG threshold increases with optical density (Figure 6c). Moreover, the temperature dependence study of 4 ML CdSe NPLs dispersed in poly(maleic anhydride-*alt*-1-octadecene) shows that the OG threshold at room temperature (298 K) is ∼4-fold lower than that at 4K (Figure 6d).

The measured OG threshold fluence (I_{th}, energy per unit excited area per pulse) is related to the average exciton number per NPL at the OG threshold (m_{th}):[21,57]

$$I_{th} = m_{th}\frac{h\nu}{\varepsilon S_{NPL}}\frac{OD}{1-10^{-OD}} = \frac{2h\nu}{\varepsilon S_X}\frac{m_{th}}{N_S}\frac{OD}{1-10^{-OD}} \quad (3)$$

In eq 3, $h\nu$ is the pump photon energy (3.1 eV), N_{NPL} is the number of NPLs per unit volume. $OD = \varepsilon V_{NPL} N_{NPL} L$ is the optical density at the pump wavelength, ε is the single NPL extinction coefficient per unit NPL volume, L = 1 mm is the

DOI: 10.1021/acs.accounts.9b00252
Acc. Chem. Res. 2019, 52, 2684−2693

sample thickness, and S_{NPL} is the NPL lateral area. S_X is the exciton coherent area, and N_S is the saturation number of band-edge excitons (Section 4). Eq 3 predicts that, for the same NPL at room temperature, I_{th} only increases with the optical density, which is confirmed by the excellent fits of optical density dependent OG threshold by eq 3 (red line in Figure 6). For different NPLs with the same optical density at room temperature, I_{th} is proportional to the ratio of m_{th}/N_S according to eq 3. Because m_{th} increases linearly with N_S (inset of Figure 6d),[21] m_{th}/N_S can be considered as a constant, and I_{th} is independent of NPL lateral area.[57] This NPL lateral area independent OG threshold is consistent with a previous report by She et al.[55] but is inconsistent with another report by Olutas et al., who observed higher OG threshold in larger NPLs.[11]

The OG threshold in 2D NPLs has been reported to be more than an order of magnitude lower than those in 0D QDs.[7,16,17] This can be attributed to the larger absorption coefficient per unit volume of CdSe NPLs (ε) than QDs,[58] which according to eq 3 reduces OG threshold. CdSe NPLs are also reported to possess a model gain coefficient (i.e., light amplification factor per unit length) of 6600 cm^{-1} at room temperature, which is over 10-fold larger than that reported in cadmium chalcogenide QDs (150−650 cm^{-1}).[15]

Because the exciton coherent area (S_X) of a NPL increases at low temperatures (as discussed in Section 3), it reduces the saturation number of band-edge excitons (N_S) and lowers the average band-edge exciton number (m_{th}) at the OG threshold. Therefore, according to eq 3, the I_{th} value decreases at lower temperatures. This OG threshold reduction results from the extension of exciton coherent area at low temperature, which is unique to 2D NPLs. The 0D QDs are completely quantum-confined in all dimensions at all temperatures, and their coherent area is independent of temperature. In 1D cadmium chalcogenide NRs, there exist large variations of confinement energies along the NR length because of nonuniform rod diameters, which prevent coherent extension of excitons along the NR length. As a result, nearly temperature-independent OG and ASE thresholds have been reported in 0D CdSe QDs[17] and 1D CdSe/CdS NRs.[59] Although the gain threshold of bulk materials also decreases at lower temperature, its origin differs from that of 2D materials. In bulk materials, there exists an exponential absorption tail below the band gap induced by doping/defect states, and the loss caused by these states decreases at lower temperature.[60] However, the OG threshold of 2D NPLs, with a large exciton binding energy (~100 meV),[1] is determined by the relative populations of NPL species with different number of A excitons (Figure 6e). This reduction of OG threshold by the exciton coherent area extension and GOST effect provides a new strategy for the development of low-threshold lasing materials. Moreover, type-II CC NPL heterostructures have been reported to further reduce the OG threshold due to a larger biexciton interaction energy.[61,62]

7. SUMMARY AND PERSPECTIVES

In summary, this Account provides a review of recent studies on the 2D exciton structure and dynamics and their effects on the OG mechanism and threshold of cadmium chalcogenide NPLs. The exciton center-of-mass coherent area in CdSe NPLs is shown to be smaller than NPL lateral area at room temperature but can extend throughout the whole NPL at low temperature (<4K) to enable the GOST effect. Both hot and cold (band-edge) excitons transport diffusively in the plane of NPLs, and the diffusion constant of the band-edge exciton is close to that of bulk crystals, ensuring ultrafast exciton transport in these materials. Because of this fast in-plane diffusion of excitons, multiexcitons collide with each other frequently in CdSe NPLs before annihilation. The Auger recombination rate is determined by the exciton binary collision frequency and the Auger probability per collision; the former scales linearly with the inverse of the NPL lateral area and the latter increases highly nonlinearly with the inverse of NPL thicknesses. Because of these different dependences on the quantum confined and non-confined dimensions, Auger recombination rates in NPLs do not obey the "universal volume scaling law" that has been observed for quantum dots. The dependences of the OG threshold of CdSe NPLs on the NPL lateral area, optical density, and temperature are reviewed. Larger NPLs can contain more band-edge excitons, which, on one hand, increases its extinction coefficient, and on the other hand, requires more excitons to reach the OG threshold, resulting in a lateral area independent OG threshold. Interestingly, exciton coherent area extension at low temperature effectively reduces the degree of band-edge exciton degeneracy, lowering the OG thresholds.

Although promising optoelectrical performances of 2D NPLs have been reported, there remain challenges on material synthesis and further understanding of exciton properties and OG mechanisms. First, NPLs with larger lateral areas are needed to further suppress Auger recombination. However, controlling and extending lateral dimension of 2D NPLs are still challenging, and larger NPLs usually have more defect/trap states and lower PL quantum yields. Second, although it is shown that the exciton center-of-mass coherent area can be extended at low temperature to significantly decrease the optical gain threshold, achieving the same goal at the room temperature remains a challenge. Exciton center-of-mass coherent area is smaller than the estimated value if only exciton−phonon scattering is considered, suggesting the presence of yet-to-be-identified scattering/dephasing pathways. One possible factor is the inhomogeneity of the interaction between the surface capping ligand and NPL.[63,64] It is thus important to develop synthetic methods that can reduce this spatial heterogeneity. It has also been shown that exciton center-of-mass coherent area increases in thinner NPLs. Thus, thinner NPLs may be promising candidates for achieving even lower room temperature lasing thresholds. Finally, most studies of NPL materials are focused on cadimum chalcogenide and how the properties of exciton spatial coherence, transport, and Auger recombination depend on material composition remains an open question.

AUTHOR INFORMATION

Corresponding Author

*E-mail: tlian@emory.edu.

ORCID

Qiuyang Li: 0000-0002-8192-3960

Tianquan Lian: 0000-0002-8351-3690

Funding

The authors gratefully acknowledge the financial support from the National Science Foundation (CHE-1709182).

Notes

The authors declare no competing financial interest.

DOI: 10.1021/acs.accounts.9b00252
Acc. Chem. Res. 2019, 52, 2684−2693

Biographies

Qiuyang Li received his B.S. in materials physics from the University of Science and Technology of China and Ph.D. in physical chemistry from Emory University advised by Prof. Tianquan (Tim) Lian. His research is focused on ultrafast carrier dynamics in two-dimensional semiconductor nanoplatelets.

Tianquan (Tim) Lian received his B.S. from Xiamen University, M.S. from the Chinese Academy of Sciences, and Ph.D. from the University of Pennsylvania. After postdoctoral training in the University of California at Berkeley, he joined the faculty of chemistry department at Emory University in 1996. He is currently the William Henry Emerson Professor in chemistry. Prof. Lian's research interest is focused on ultrafast dynamics in photovoltaic and photocatalytic nanomaterials and at their interfaces.

REFERENCES

(1) Ithurria, S.; Tessier, M. D.; Mahler, B.; Lobo, R. P. S. M.; Dubertret, B.; Efros, A. Colloidal nanoplatelets with two-dimensional electronic structure. *Nat. Mater.* **2011**, *10*, 936−941.

(2) Nasilowski, M.; Mahler, B.; Lhuillier, E.; Ithurria, S.; Dubertret, B. Two-Dimensional Colloidal Nanocrystals. *Chem. Rev.* **2016**, *116*, 10934−10982.

(3) Tessier, M. D.; Javaux, C.; Maksimovic, I.; Loriette, V.; Dubertret, B. Spectroscopy of Single CdSe Nanoplatelets. *ACS Nano* **2012**, *6*, 6751−6758.

(4) Chen, O.; Zhao, J.; Chauhan, V. P.; Cui, J.; Wong, C.; Harris, D. K.; Wei, H.; Han, H.-S.; Fukumura, D.; Jain, R. K.; Bawendi, M. G. Compact High-quality CdSe−CdS Core−Shell Nanocrystals with Narrow Emission Linewidths and Suppressed Blinking. *Nat. Mater.* **2013**, *12*, 445−451.

(5) Singh, S.; Tomar, R.; ten Brinck, S.; De Roo, J.; Geiregat, P.; Martins, J. C.; Infante, I.; Hens, Z. Colloidal CdSe Nanoplatelets, A Model for Surface Chemistry/Optoelectronic Property Relations in Semiconductor Nanocrystals. *J. Am. Chem. Soc.* **2018**, *140*, 13292−13300.

(6) Li, Q.; Lian, T. Area- and Thickness-Dependent Biexciton Auger Recombination in Colloidal CdSe Nanoplatelets: Breaking the "Universal Volume Scaling Law. *Nano Lett.* **2017**, *17*, 3152−3158.

(7) Grim, J. Q.; Christodoulou, S.; Di Stasio, F.; Krahne, R.; Cingolani, R.; Manna, L.; Moreels, I. Continuous-wave biexciton lasing at room temperature using solution-processed quantum wells. *Nat. Nanotechnol.* **2014**, *9*, 891−895.

(8) Klimov, V. I.; Mikhailovsky, A. A.; McBranch, D. W.; Leatherdale, C. A.; Bawendi, M. G. Quantization of multiparticle Auger rates in semiconductor quantum dots. *Science* **2000**, *287*, 1011−1013.

(9) Guzelturk, B.; Kelestemur, Y.; Olutas, M.; Delikanli, S.; Demir, H. V. Amplified Spontaneous Emission and Lasing in Colloidal Nanoplatelets. *ACS Nano* **2014**, *8*, 6599−6605.

(10) She, C. X.; Fedin, I.; Dolzhnikov, D. S.; Demortiere, A.; Schaller, R. D.; Pelton, M.; Talapin, D. V. Low-Threshold Stimulated Emission Using Colloidal Quantum Wells. *Nano Lett.* **2014**, *14*, 2772−2777.

(11) Olutas, M.; Guzelturk, B.; Kelestemur, Y.; Yeltik, A.; Delikanli, S.; Demir, H. V. Lateral Size-Dependent Spontaneous and Stimulated Emission Properties in Colloidal CdSe Nanoplatelets. *ACS Nano* **2015**, *9*, 5041−5050.

(12) Li, Q.; Xu, Z.; McBride, J. R.; Lian, T. Low Threshold Multiexciton Optical Gain in Colloidal CdSe/CdTe Core/Crown Type-II Nanoplatelet Heterostructures. *ACS Nano* **2017**, *11*, 2545−2553.

(13) Yang, Z.; Pelton, M.; Fedin, I.; Talapin, D. V.; et al. Waks, E. A room temperature continuous-wave nanolaser using colloidal quantum wells. *Nat. Commun.* **2017**, *8*, 143.

(14) Pelton, M. Carrier Dynamics, Optical Gain, and Lasing with Colloidal Quantum Wells. *J. Phys. Chem. C* **2018**, *122*, 10659−10674.

(15) Guzelturk, B.; Pelton, M.; Olutas, M.; Demir, H. V. Giant Modal Gain Coefficients in Colloidal II-VI Nanoplatelets. *Nano Lett.* **2019**, *19*, 277−282.

(16) Klimov, V. I.; Ivanov, S. A.; Nanda, J.; Achermann, M.; Bezel, I.; McGuire, J. A.; Piryatinski, A. Single-exciton Optical Gain in Semiconductor Nanocrystals. *Nature* **2007**, *447*, 441−446.

(17) Klimov, V.; Mikhailovsky, A.; Xu, S.; Malko, A.; Hollingsworth, J.; Leatherdale, C.; Eisler, H. J.; Bawendi, M. Optical gain and stimulated emission in nanocrystal quantum dots. *Science* **2000**, *290*, 314−317.

(18) Benchamekh, R.; Gippius, N. A.; Even, J.; Nestoklon, M. O.; Jancu, J. M.; Ithurria, S.; Dubertret, B.; Efros, A. L.; Voisin, P. Tight-binding calculations of image-charge effects in colloidal nanoscale platelets of CdSe. *Phys. Rev. B: Condens. Matter Mater. Phys.* **2014**, *89*, No. 035307.

(19) Feldmann, J.; Peter, G.; Göbel, E. O.; Dawson, P.; Moore, K.; Foxon, C.; Elliott, R. J. Linewidth dependence of radiative exciton lifetimes in quantum wells. *Phys. Rev. Lett.* **1987**, *59*, 2337−2340.

(20) Naeem, A.; Masia, F.; Christodoulou, S.; Moreels, I.; Borri, P.; Langbein, W. Giant exciton oscillator strength and radiatively limited dephasing in two-dimensional platelets. *Phys. Rev. B: Condens. Matter Mater. Phys.* **2015**, *91*, 121302.

(21) Li, Q.; Liu, Q.; Schaller, R. D.; Lian, T. Reducing the Optical Gain Threshold in Two-Dimensional CdSe Nanoplatelets by the Giant Oscillator Strength Transition Effect. *J. Phys. Chem. Lett.* **2019**, *10*, 1624−1632.

(22) Ma, X.; Diroll, B. T.; Cho, W.; Fedin, I.; Schaller, R. D.; Talapin, D. V.; Gray, S. K.; Wiederrecht, G. P.; Gosztola, D. J. Size-Dependent Biexciton Quantum Yields and Carrier Dynamics of Quasi-Two-Dimensional Core/Shell Nanoplatelets. *ACS Nano* **2017**, *11*, 9119−9127.

(23) Li, Q.; Wu, K.; Chen, J.; Chen, Z.; McBride, J. R.; Lian, T. Size-Independent Exciton Localization Efficiency in Colloidal CdSe/CdS Core/Crown Nanosheet Type-I Heterostructures. *ACS Nano* **2016**, *10*, 3843−3851.

(24) Li, Q.; Zhou, B.; McBride, J. R.; Lian, T. Efficient Diffusive Transport of Hot and Cold Excitons in Colloidal Type II CdSe/CdTe Core/Crown Nanoplatelet Heterostructures. *ACS Energy Letters* **2017**, *2*, 174−181.

(25) Kunneman, L. T.; Tessier, M. D.; Heuclin, H.; Dubertret, B.; Aulin, Y. V.; Grozema, F. C.; Schins, J. M.; Siebbeles, L. D. A. Bimolecular Auger Recombination of Electron-Hole Pairs in Two-Dimensional CdSe and CdSe/CdZnS Core/Shell Nanoplatelets. *J. Phys. Chem. Lett.* **2013**, *4*, 3574−3578.

(26) Tessier, M. D.; Spinicelli, P.; Dupont, D.; Patriarche, G.; Ithurria, S.; Dubertret, B. Efficient Exciton Concentrators Built from Colloidal Core/Crown CdSe/CdS Semiconductor Nanoplatelets. *Nano Lett.* **2014**, *14*, 207−213.

(27) Wu, K.; Li, Q.; Jia, Y.; McBride, J. R.; Xie, Z.-x.; Lian, T. Efficient and Ultrafast Formation of Long-Lived Charge-Transfer Exciton State in Atomically Thin Cadmium Selenide/Cadmium Telluride Type-II Heteronanosheets. *ACS Nano* **2015**, *9*, 961−968.

(28) Kelestemur, Y.; Olutas, M.; Delikanli, S.; Guzelturk, B.; Akgul, M. Z.; Demir, H. V. Type-II Colloidal Quantum Wells: CdSe/CdTe Core/Crown Heteronanoplatelets. *J. Phys. Chem. C* **2015**, *119*, 2177−2185.

(29) Pedetti, S.; Ithurria, S.; Heuclin, H.; Patriarche, G.; Dubertret, B. Type-II CdSe/CdTe Core/Crown Semiconductor Nanoplatelets. *J. Am. Chem. Soc.* **2014**, *136*, 16430−16438.

(30) Diroll, B. T.; Fedin, I.; Darancet, P.; Talapin, D. V.; Schaller, R. D. Surface-Area-Dependent Electron Transfer Between Isoenergetic 2D Quantum Wells and a Molecular Acceptor. *J. Am. Chem. Soc.* **2016**, *138*, 11109−11112.

(31) Luer, L.; Hoseinkhani, S.; Polli, D.; Crochet, J.; Hertel, T.; Lanzani, G. Size and mobility of excitons in (6, 5) carbon nanotubes. *Nat. Phys.* **2009**, *5*, 54−58.

(32) Chernikov, A.; Berkelbach, T. C.; Hill, H. M.; Rigosi, A.; Li, Y.; Aslan, O. B.; Reichman, D. R.; Hybertsen, M. S.; Heinz, T. F. Exciton

DOI: 10.1021/acs.accounts.9b00252
Acc. Chem. Res. 2019, 52, 2684−2693

Binding Energy and Nonhydrogenic Rydberg Series in Monolayer WS2. *Phys. Rev. Lett.* **2014**, *113*, No. 076802.
(33) Wu, K.; Li, Q.; Du, Y.; Chen, Z.; Lian, T. Ultrafast exciton quenching by energy and electron transfer in colloidal CdSe nanosheet-Pt heterostructures. *Chemical Science* **2015**, *6*, 1049−1054.
(34) Li, Q.; Zhao, F.; Qu, C.; Shang, Q.; Xu, Z.; Yu, L.; McBride, J. R.; Lian, T. Two-Dimensional Morphology Enhances Light-Driven H2 Generation Efficiency in CdS Nanoplatelet-Pt Heterostructures. *J. Am. Chem. Soc.* **2018**, *140*, 11726−11734.
(35) Li, Q.; Lian, T. Exciton dissociation dynamics and light-driven H2 generation in colloidal 2D cadmium chalcogenide nanoplatelet heterostructures. *Nano Res.* **2018**, *11*, 3031−3049.
(36) Zhukovskyi, M.; Tongying, P.; Yashan, H.; Wang, Y.; Kuno, M. Efficient Photocatalytic Hydrogen Generation from Ni Nanoparticle Decorated CdS Nanosheets. *ACS Catal.* **2015**, *5*, 6615−6623.
(37) Liu, Y.-H.; Wayman, V. L.; Gibbons, P. C.; Loomis, R. A.; Buhro, W. E. Origin of High Photoluminescence Efficiencies in CdSe Quantum Belts. *Nano Lett.* **2010**, *10*, 352−357.
(38) Zhao, H.; Moehl, S.; Kalt, H. Coherence Length of Excitons in a Semiconductor Quantum Well. *Phys. Rev. Lett.* **2002**, *89*, No. 097401.
(39) Zhao, H.; Moehl, S.; Wachter, S.; Kalt, H. Hot exciton transport in ZnSe quantum wells. *Appl. Phys. Lett.* **2002**, *80*, 1391−1393.
(40) Zhao, H.; Dal Don, B.; Moehl, S.; Kalt, H.; Ohkawa, K.; Hommel, D. Spatiotemporal dynamics of quantum-well excitons. *Phys. Rev. B: Condens. Matter Mater. Phys.* **2003**, *67*, No. 035306.
(41) Kalt, H.; Zhao, H.; Don, B. D.; Schwartz, G.; Bradford, C.; Prior, K. Quasi-ballistic transport of excitons in quantum wells. *J. Lumin.* **2005**, *112*, 136−141.
(42) Wu, K.; Hill, L. J.; Chen, J.; McBride, J. R.; Pavlopolous, N. G.; Richey, N. E.; Pyun, J.; Lian, T. Universal Length Dependence of Rod-to-Seed Exciton Localization Efficiency in Type I and Quasi-Type II CdSe@CdS Nanorods. *ACS Nano* **2015**, *9*, 4591−4599.
(43) Pandya, R.; Chen, R. Y. S.; Cheminal, A.; Dufour, M.; Richter, J. M.; Thomas, T. H.; Ahmed, S.; Sadhanala, A.; Booker, E. P.; Divitini, G.; Deschler, F.; Greenham, N. C.; Ithurria, S.; Rao, A. Exciton−Phonon Interactions Govern Charge-Transfer-State Dynamics in CdSe/CdTe Two-Dimensional Colloidal Heterostructures. *J. Am. Chem. Soc.* **2018**, *140*, 14097−14111.
(44) Liu, B.; Delikanli, S.; Gao, Y.; Dede, D.; Gungor, K.; Demir, H. V. Nanocrystal light-emitting diodes based on type II nanoplatelets. *Nano Energy* **2018**, *47*, 115−122.
(45) Giovanella, U.; Pasini, M.; Lorenzon, M.; Galeotti, F.; Lucchi, C.; Meinardi, F.; Luzzati, S.; Dubertret, B.; Brovelli, S. Efficient Solution-Processed Nanoplatelet-Based Light-Emitting Diodes with High Operational Stability in Air. *Nano Lett.* **2018**, *18*, 3441−3448.
(46) Zhu, H. M.; Yang, Y.; Lian, T. Q. Multiexciton Annihilation and Dissociation in Quantum Confined Semiconductor Nanocrystals. *Acc. Chem. Res.* **2013**, *46*, 1270−1279.
(47) Robel, I.; Gresback, R.; Kortshagen, U.; Schaller, R. D.; Klimov, V. I. Universal Size-Dependent Trend in Auger Recombination in Direct-Gap and Indirect-Gap Semiconductor Nanocrystals. *Phys. Rev. Lett.* **2009**, *102*, 177404.
(48) Padilha, L. A.; Stewart, J. T.; Sandberg, R. L.; Bae, W. K.; Koh, W.-K.; Pietryga, J. M.; Klimov, V. I. Aspect Ratio Dependence of Auger Recombination and Carrier Multiplication in PbSe Nanorods. *Nano Lett.* **2013**, *13*, 1092−1099.
(49) Pelton, M.; Andrews, J. J.; Fedin, I.; Talapin, D. V.; Leng, H.; O'Leary, S. K. Nonmonotonic Dependence of Auger Recombination Rate on Shell Thickness for CdSe/CdS Core/Shell Nanoplatelets. *Nano Lett.* **2017**, *17*, 6900−6906.
(50) Robel, I.; Gresback, R.; Kortshagen, U.; Schaller, R. D.; Klimov, V. I. Universal Size-Dependent Trend in Auger Recombination in Direct-Gap and Indirect-Gap Semiconductor Nanocrystals. *Phys. Rev. Lett.* **2009**, *102*, 177404.
(51) Lim, J.; Park, Y.-S.; Klimov, V. I. Optical gain in colloidal quantum dots achieved with direct-current electrical pumping. *Nat. Mater.* **2018**, *17*, 42−49.
(52) Wang, F.; Wu, Y.; Hybertsen, M. S.; Heinz, T. F. Auger recombination of excitons in one-dimensional systems. *Phys. Rev. B: Condens. Matter Mater. Phys.* **2006**, *73*, 2452424.
(53) Vaxenburg, R.; Rodina, A.; Shabaev, A.; Lifshitz, E.; Efros, A. L. Nonradiative Auger Recombination in Semiconductor Nanocrystals. *Nano Lett.* **2015**, *15*, 2092−2098.
(54) Li, Q.; Yang, Y.; Que, W.; Lian, T. Size- and Morphology-Dependent Auger Recombination in CsPbBr3 Perovskite Two-Dimensional Nanoplatelets and One-Dimensional Nanorods. *Nano Lett.* **2019**, DOI: 10.1021/acs.nanolett.9b02145.
(55) She, C.; Fedin, I.; Dolzhnikov, D. S.; Dahlberg, P. D.; Engel, G. S.; Schaller, R. D.; Talapin, D. V. Red, Yellow, Green, and Blue Amplified Spontaneous Emission and Lasing Using Colloidal CdSe Nanoplatelets. *ACS Nano* **2015**, *9*, 9475−9485.
(56) Philbin, J. P.; Rabani, E. Electron−Hole Correlations Govern Auger Recombination in Nanostructures. *Nano Lett.* **2018**, *18*, 7889−7895.
(57) Li, Q.; Lian, T. A model for optical gain in colloidal nanoplatelets. *Chemical Science* **2018**, *9*, 728−734.
(58) Achtstein, A. W.; Antanovich, A.; Prudnikau, A.; Scott, R.; Woggon, U.; Artemyev, M. Linear Absorption in CdSe Nanoplates: Thickness and Lateral Size Dependency of the Intrinsic Absorption. *J. Phys. Chem. C* **2015**, *119*, 20156−20161.
(59) Moreels, I.; Raino, G.; Gomes, R.; Hens, Z.; Stoferle, T.; Mahrt, R. F. Nearly Temperature-Independent Threshold for Amplified Spontaneous Emission in Colloidal CdSe/CdS Quantum Dot-in-Rods. *Adv. Mater.* **2012**, *24*, OP231−OP235.
(60) Pankove, J. Temperature dependence of emission efficiency and lasing threshold in laser diodes. *IEEE J. Quantum Electron.* **1968**, *4*, 119−122.
(61) Dede, D.; Taghipour, N.; Quliyeva, U.; Sak, M.; Kelestemur, Y.; Gungor, K.; Demir, H. V. Highly Stable Multi-Crown Heterostructures of Type-II Nanoplatelets for Ultra-Low Threshold Optical Gain. *Chem. Mater.* **2019**, *31*, 1818−1826.
(62) Guzelturk, B.; Kelestemur, Y.; Olutas, M.; Li, Q.; Lian, T.; Demir, H. V. High-Efficiency Optical Gain in Type-II Semiconductor Nanocrystals of Alloyed Colloidal Quantum Wells. *J. Phys. Chem. Lett.* **2017**, *8*, 5317−5324.
(63) Rodina, A. V.; Golovatenko, A. A.; Shornikova, E. V.; Yakovlev, D. R.; Efros, A. L. Effect of Dangling Bond Spins on the Dark Exciton Recombination and Spin Polarization in CdSe Colloidal Nanostructures. *J. Electron. Mater.* **2018**, *47*, 4338−4344.
(64) Mack, T. G.; Jethi, L.; Andrews, M. P.; Kambhampati, P. Direct Observation of Electronic Mixing Excitonic States of Nanocrystals and Their Passivating Ligands. *J. Phys. Chem. C* **2019**, *123*, 5084−5091.

DOI: 10.1021/acs.accounts.9b00252
Acc. Chem. Res. 2019, 52, 2684−2693